Detection and Localization of Submodule Open-Circuit Failures for Modular Multilevel Converters With Single Ring Theorem

Weihao Zhou, Jing Sheng, Haoze Luo, *Member, IEEE*, Wuhua Li, *Member, IEEE*, and Xiangning He, *Fellow, IEEE*

***Abstract*—Submodule (SM) failure detection and localization is crucial to reliability improvement of modular multilevel converters (MMCs), which consist of numerous identical SMs. Upon SM failures, the capacitor voltages of the faulty SMs deviate from those of the healthy SMs. Hence, SM voltage consistency disruption can be utilized as an indicator of SM failures. To enable effective consistency evaluation of numerous SM voltages, the single ring theorem, which is an ideal analyzing tool for large size matrices, is applied to SM failure detection in this paper. The proposed SM failure detection method eliminates the need for ideal-state estimators and thus ensures sufficient robustness in terms of parameter uncertainties. Additional voltage/current sensors are not required, which is beneficial for cost efficiency. A statistical-analysis-based SM failure localization method enabling fast identification of the faulty SMs upon failure detection is also proposed. Both single and multiple SM failure detection and localization can be handled with the proposed method even if the faulty SMs are in different arms. The effectiveness of the proposed SM failure diagnosis method is verified by both simulation in MATLAB/Simulink and experimentation on a 13-level MMC prototype.**

***Index Terms*—Fault detection, fault localization, modular multilevel converters, single ring theorem.**

I. Introduction

MODULAR multilevel converters (MMCs) are gaining increasing usage in high-voltage and high-power applications [1]–[3]. Unlike the traditional two-level or multilevel converters, numerous submodules (SMs) are series connected in the MMC [4]–[7]. The application of series-connected SMs reduces the demand on signal synchronization while also ensuring high ac supply quality, flexibility, and modularity [8]–[11]. However, the application of many SMs poses challenges to the reliability of MMCs. Multiple power switching devices are embedded within each SM and are more prone to failure than

Manuscript received April 4, 2018; revised May 14, 2018; accepted June 6, 2018. Date of publication June 20, 2018; date of current version February 20, 2019. This work was supported in part by the National Natural Science Foundations of China under Grants 51490682 and 51677166, in part by the National Basic Research Program of China (973 Program) under Grant 2014CB247400, and in part by Zhejiang Provincial Natural Science Foundation (LR16E070001). Recommended for publication by Associate Editor M. Hagiwara. *(Corresponding author: Wuhua Li.)*

The authors are with the College of Electrical Engineering, Zhejiang University, Hangzhou 310027, China (e-mail:

with the single ring theorem (SRT) in this paper. The SRT studies the property of large size random matrices and has been applied to operating status evaluation and fault recognition in power systems [23], [24]. Once the matrix size is sufficiently large and all matrix elements are independent identically distributed (IID), the eigenvalues of the analyzed matrix tend to scatter within a dedicated single ring in the complex plane. However, the eigenvalue distribution breaks the single ring once the IID property of the matrix elements is disrupted [25], [26]. A random matrix construction strategy based on SM voltages is proposed in this paper. By applying the SRT to the constructed random matrix, SM open-circuit failures can be correctly detected. A faulty SM localization method is then activated upon SM failure detection. The localization method identifies the faulty SMs based on the concept of outlier recognition in statistical analysis. The proposed failure diagnosis method requires no additional sensors and thus introduces no extra cost. No estimator is utilized which aids the robustness of the method since parameter uncertainties exert negligible impact on the diagnosis effectiveness. The proposed method is capable of dealing with both single and multiple SM failures even if the faulty SMs are located in different arms. The feasibility of the proposed SM open-circuit failure diagnosis method is verified by simulation results on a detailed 61-level MMC model in MATLAB/Simulink and experimental results on a 13-level MMC prototype.

The remainder of the paper is organized as follows. The fault characteristics of MMCs under SM open-circuit failures are analyzed in Section II. The proposed SM failure detection and faulty SM localization methods are introduced in Section III. In Sections IV and V, simulation results and experimental results are presented to validate the effectiveness of the proposed SM failure diagnosis method. Finally, conclusions drawn from the investigation are presented in Section VI.

II. Fault Characteristics of SM Open-Circuit Failures

In this section, the fault characteristics of MMCs under SM open-circuit failures are analyzed to provide the prior knowledge for SM failure diagnosis in later sections. The basic diagram of a three-phase MMC based on half-bridge SMs (HBSMs) is depicted in Fig. 1. A total number of six identical arms (two per phase: positive arm and negative arm) are included in an MMC. A series of HBSMs and an inductor $L_{\rm Arm}$ are equipped within each arm. The detailed operation principles of MMCs have been elaborated in [27] and will not be presented here. SM open-circuit failures can be categorized into three types, S_u open-circuit failures, S_l open-circuit failures, and S_u & S_l open-circuit failures, depending upon distinct failure points as shown in Fig. 2. The fault characteristics would be analyzed separately for the three failure types and the analysis is conducted based on the reference directions defined in Fig. 1.

A. S_u Open-Circuit Failure

The fault characteristics of S_u open-circuit failures are presented in Table I. S_u open-circuit failures have no impact on MMC operation once the SM current $i_{\rm SM}$ is positive. However, a negative SM current flows through D_l whether a faulty SM is required to be inserted or bypassed. In this case, a faulty SM loses the ability to discharge. The capacitor voltage of a faulty SM remains at the highest value ever reached with notable deviation from healthy SMs.

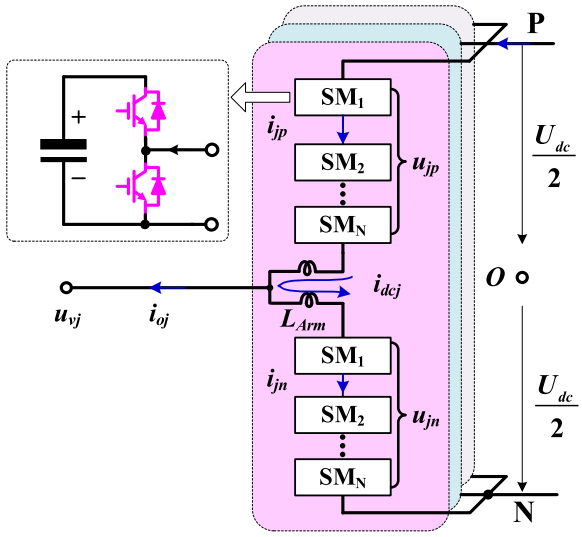

Fig. 1. Basic diagram of three-phase MMCs with HBSMs.

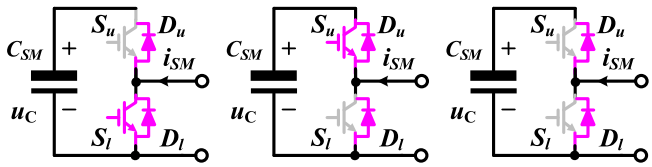

Fig. 2. Three types of SM open-circuit failures. (a) S_u open-circuit failure. (b) S_l open-circuit failure. (c) S_u & S_l open-circuit failure.

TABLE I
Fault Characteristics of S_u Open-Circuit Failure

SM current direction	Command	Current path and SM voltage variation			
		Normal operation		S_u open-circuit failure	
Positive	Insert	D_u & C_{SM}	Charging	D_u & C_{SM}	Charing
	Bypass	S_l	Unchanged	S_l	Unchanged
Negative	Insert	S_u & C_{SM}	Discharging	D_l	Unchanged
	Bypass	D_l	Unchanged	D_l	Unchanged

TABLE II
Fault Characteristics of S_l Open-Circuit Failure

SM current direction	Command	Current path and SM voltage variation			
		Normal operation		S_u open-circuit failure	
Positive	Insert	D_u & C_{SM}	Charging	D_u & C_{SM}	Charing
	Bypass	S_l	Unchanged	D_u & C_{SM}	Charing
Negative	Insert	S_u & C_{SM}	Discharging	S_u & C_{SM}	Discharging
	Bypass	D_l	Unchanged	D_l	Unchanged

B. S_l Open-Circuit Failure

The fault characteristics of S_l open-circuit failures are presented in Table II. As opposed to S_u open-circuit failures, S_l open-circuit failures have no impact on MMC operation if $i_{\rm SM}$ is negative. However, a positive SM current is forced to flow through D_u regardless of the SM action command (insert or bypass) and charges the dc capacitor continuously. Therefore, a

TABLE III
FAULT CHARACTERISTICS OF S_u & S_l OPEN-CIRCUIT FAILURE

SM current direction	Command	Current path and SM voltage variation			
		Normal operation		S_u open-circuit failure	
Positive	Insert	D_u & C_{SM}	Charging	D_u & C_{SM}	Charing
	Bypass	S_l	Unchanged	D_u & C_{SM}	Charing
Negative	Insert	S_u & C_{SM}	Discharging	D_l	Unchanged
	Bypass	D_l	Unchanged	D_l	Unchanged

faulty SM has one more extra charging period than normal SMs, leading to a higher capacitor voltage.

C. S_u & S_l Open-Circuit Failure

The fault characteristics of S_u & S_l open-circuit failures are presented in Table III. S_u & S_l open-circuit failures can be regarded as an integration of S_u open-circuit failures and S_l open-circuit failures. In other words, a faulty SM loses the ability to discharge while having one more extra charging period than healthy SMs. Hence, a faulty SM has a higher capacitor voltage than healthy SMs eventually.

In summary, the SM capacitor voltage of a faulty SM deviates from those of normal SMs under all types of SM open-circuit failures. This property forms the basis of the SM failure diagnosis method to be proposed.

III. PROPOSED SM FAILURE DIAGNOSIS METHOD

In this section, the proposed SM failure diagnosis method is elaborated. First, a general introduction of the SRT is given. The SM failure detection method based on the SRT is introduced then, where a random matrix construction method based on SM capacitor voltages is proposed. The SM failure localization method is presented in the end.

A. Single Ring Theorem

SRT studies the empirical spectral distribution of a random matrix's eigenvalues. For a $N \times T$ ($N/T \in (0, 1]$) non-Hermitian matrix $\mathbf{X}$, the conversion shown in (1) is first taken to transfer it into a standard non-Hermitian matrix $\tilde{\mathbf{X}}$. $\mu(\mathbf{x}_i)$ and $\sigma(\mathbf{x}_i)$ refer to the expectation and standard deviation of the ith row vector in $\mathbf{X}$, respectively

$$\tilde{\mathbf{x}}_{i,j} = (x_{i,j} - \mu(\mathbf{x}_i))/\sigma(\mathbf{x}_i). \tag{1}$$

The singular value equivalent matrix $\hat{\mathrm{X}}u$ is then derived by the following equation:

$$\hat{\mathbf{X}}_u = \sqrt{\tilde{\mathbf{X}}\tilde{\mathbf{X}}^H}\mathbf{U} \tag{2}$$

where $\mathbf{U}$ is an $N \times N$ Haar unitary matrix and $\tilde{\mathbf{X}}_u\tilde{\mathbf{X}}_u^H = \tilde{\mathbf{X}}\tilde{\mathbf{X}}^{\mathrm{H}}$.

Finally, the standard matrix $\mathbf{Z}$ is acquired through the following equation:

$$\mathbf{z}_i = \frac{\tilde{\mathbf{X}}_{u,i}}{\sqrt{N}\sigma(\tilde{\mathbf{x}}_{u,i})} \tag{3}$$

where $\mathbf{z}_i$ and $\tilde{\mathbf{x}}_{u,i}$ denote the i^{th} row vector of $\mathbf{Z}$ and $\tilde{\mathbf{X}}_u$, respectively. The elements in $\mathbf{Z}$ satisfy $\mu(z_{i,j}) = 0$ and $\sigma^2(z_{i,j}) = 1/N$.

It has been proved [25] that once all elements in $\mathbf{X}$ are independent identically distributed (IID), the eigenvalue distribution

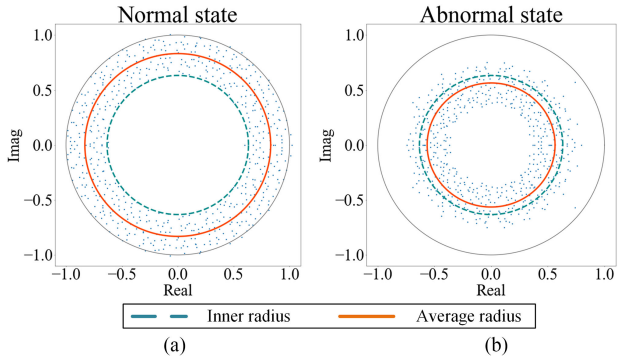

Fig. 3. Eigenvalue distribution of matrix Z.

of $\mathbf{Z}$ tends to obey the probability distribution function (PDF) given in (4) as N and T approaches infinity. That is, all eigenvalues $(\lambda_1, \lambda_2, \ldots, \lambda_N)$ of $\mathbf{Z}$ scatter within a circle with an inner radius of $(1 - N/T)^2$ and an outer radius of 1 (normal state). However, the eigenvalue distribution breaks through the inner radius once the IID property of the matrix elements are spoiled (abnormal state). As an example, the eigenvalue distribution of a 600×1000 random matrix under normal and abnormal states is depicted in Fig. 3. Outliers may appear once N and T are finite with negligible impact

$$f(\lambda) = \begin{cases} \frac{T}{N\pi}|\lambda|, & \left(1 - \frac{N}{T}\right)^2 \le |\lambda| \le 1 \\ 0, & \text{otherwise.} \end{cases} \tag{4}$$

The PDF of the eigenvalue radius r ($r = |\lambda|$) can be derived as follows:

$$f(r) = \begin{cases} \frac{2T}{N}r, & \left(1 - \frac{N}{T}\right)^2 \le r \le 1 \\ 0, & \text{otherwise.} \end{cases} \tag{5}$$

The mean spectral radius (MSR) shown in (6) is applied as a representative of the eigenvalue distribution

$$r_{\text{MSR}} = \frac{1}{N}\sum_{i=1}^{N}|\lambda_i|. \tag{6}$$

The drawn r_{MSR} is then compared with a preset threshold value r_{th}. Once $r_{\text{MSR}} < r_{\text{th}}$, the evaluated system is regarded to be operating abnormally. Determination of r_{th} can rely on $\mu(f(r))$—the expectation of $f(r)$. Since limited N and T are applied actually, a modifying index ε is utilized for adjustment in the following equation:

$$r_{\text{th}} = \varepsilon \cdot \mu(f(r)) = \frac{2\varepsilon T}{3N}\left[1 - \left(1 - \frac{N}{T}\right)^{1.5}\right]. \tag{7}$$

B. SM Failure Detection Method Based on SRT

The proposed diagnosis method applies the SRT to SM open-circuit failure detection. The key to the proposed detection method is random matrix construction. To enable reliable performance, the elements in the applied random matrix must meet the property of IID under normal operation and otherwise upon SM open-circuit failures. Since SM open-circuit failures have notable impact on SM capacitor voltages as shown in the last section, SM capacitor voltages are used as the origin for random

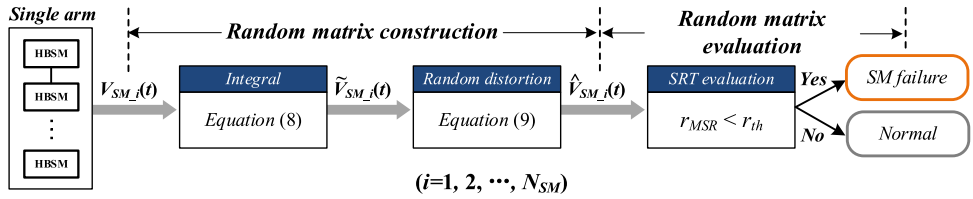

Fig. 4. Schematic representation of the proposed SM failure detection method.

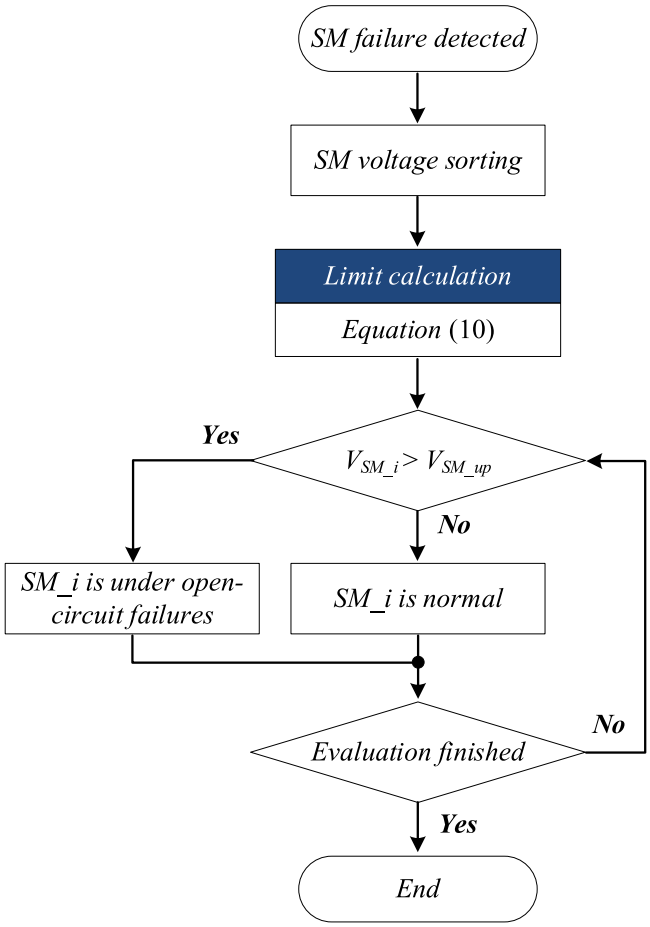

Fig. 5. Flowchart of the proposed SM failure localization method.

matrix elements. It is inappropriate to apply SM voltages directly in random matrix generation. Deviation bands inevitably exist among SM capacitor voltages within one arm even under normal operation due to a finite switching frequency [22]. Since different number of SMs are inserted at each instant, such deviation bands vary from time to time. This will cause nonideal oscillation of r_{MSR}. To address this issue, integral operation is initially taken on SM voltages. A total number of f/f_s samples are required for integral calculation, where f is the grid frequency and f_s is the sampling frequency. A queue with length f/f_s is utilized to store the sampling values. It is updated once a new sampling value is acquired by popping the first sampling value (oldest) and inserting the new sampling value at the end of the queue. The integral operation transfers SM voltages into dc quantities under normal operation as shown in (8) and thus eliminates the impact of deviation band variation. U_{c0}, U_{c1}, and U_{c2} represent the amplitude of the dc component, the fundamental frequency component, and the double-fundamental-frequency component. φ_1 and φ_2 are the phase angles of the fundamental frequency component and the double-fundamental-frequency component. t denotes an arbitrary time point and $T = 1/f$

$$\widetilde{V}_{\mathrm{SM}\_i}(t) = \int_{t-T}^{t} V_{\mathrm{SM}\_i}(t)dt = \int_{t-T}^{t} [U_{c0} \pm U_{c1}\cos(\omega t + \varphi_1) + U_{c2}\cos(2\omega t + \varphi_2)]dt = U_{c0}T. \tag{8}$$

With the integral results, random distortion in (9) is then executed to generate random matrix elements. The random distortion is performed on per unit values of $\widetilde{V}_{\mathrm{SM}\_i}(t)$. The distortion components S_{ran} are generated based on a uniform distribution on [–r, r] through arbitrary pseudorandom number generators. The value of r should be properly selected. A longer time is required for failure detection as r increases while unreasonably large r can even lead to type II errors [28] since deviations can be buried by the distortions. Meanwhile, r should not be too small so as to ensure sufficient robustness and avoid type I errors [28]

$$\hat{V}_{\mathrm{SM}\_i}(t)_j = \frac{N_{\mathrm{SM}} \cdot \widetilde{V}_{\mathrm{SM}\_i}(t)}{\sum_i \widetilde{V}_{\mathrm{SM}\_i}(t)} + S_{\mathrm{ran}} \quad (i = i, 2, \ldots, N_{\mathrm{SM}} \quad j = 1, 2, \ldots, M). \tag{9}$$

At each sampling point, the random distortion in (9) is performed on each $\widetilde{V}_{\mathrm{SM}\_i}(t)$ for M times to generate a row vector $[\hat{V}_{\mathrm{SM}\_i}(t)_1, \hat{V}_{\mathrm{SM}\_i}(t)_2, \ldots, \hat{V}_{\mathrm{SM}\_i}(t)_M]$. By integrating all N_{SM} row vectors together, an $N_{\mathrm{SM}} \times M$ random matrix is then acquired. Under normal operation, all elements in the $N_{\mathrm{SM}} \times M$ random matrix are limited within a small range and thus approximately satisfy a common uniform distribution. On the contrary, elements in the matrix will exhibit different distribution features upon SM open-circuit failures and thus ruin the IID property.

TABLE IV
KEY PARAMETERS OF SIMULATION MODEL

Item	Description	Value
S_{rated}	Rated apparent power	120MVA
PF	Power factor	1
$u_{l\text{-}l}$	Line-line voltage (*rms*)	66kV
f	Grid frequency	50Hz
U_{dc}	Rated dc voltage	120kV
C_{SM}	SM capacitance	6mF
L_{Arm}	Arm inductance	15mH
N_{SM}	Number of SMs/arm	60
f_s	Sampling frequency	5kHz

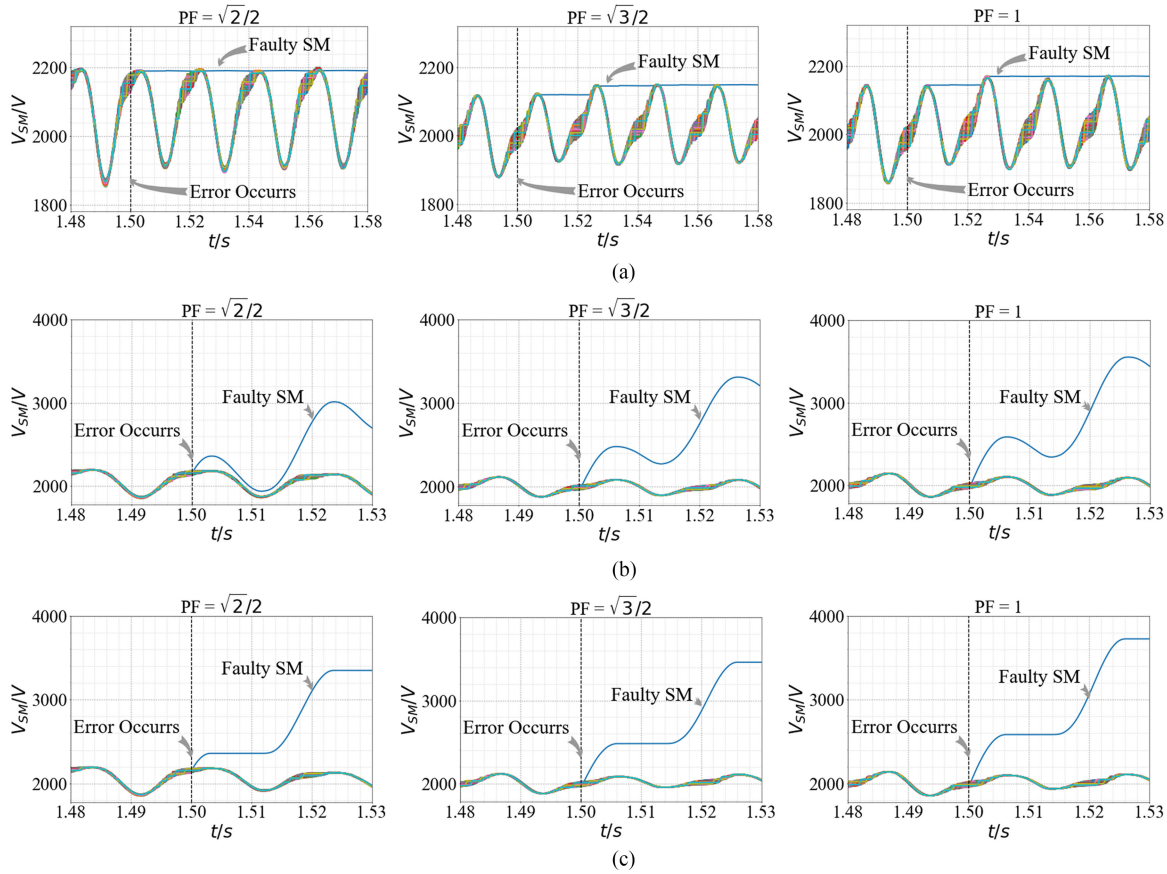

Fig. 6. Waveforms of SM capacitor voltages under different types of SM open-circuit failures. (a) S_u open-circuit failure. (b) S_l open-circuit failure. (c) S_u & S_l open-circuit failure.

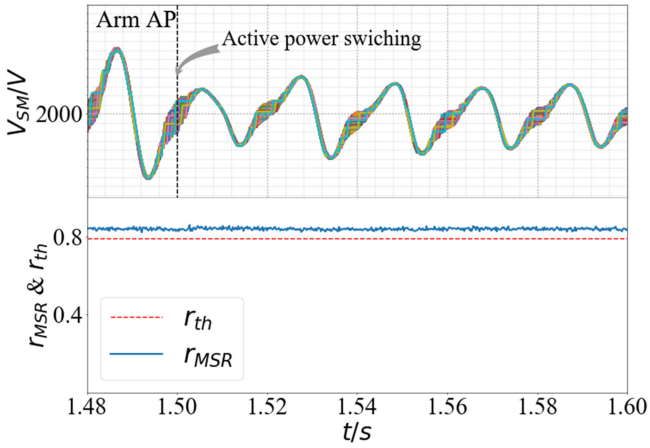

Fig. 7. Simulation result of transients under normal operation.

Based on this, r_{MSR} of the $N_{\mathrm{SM}} \times M$ random matrix is calculated through (1)–(3) and (6) at each sampling instant. Once the condition $r_{\mathrm{MSR}} < r_{\mathrm{th}}$ is met, an SM failure is assumed to happen.

The schematic representation of the proposed SM failure detection method subjected to one arm is presented in Fig. 4. In practice, all six arms in the MMC are monitored with the proposed SM failure detection method. Such a configuration enables multiple SM failure detection even if the faulty SMs are in different arms.

C. SM Failure Localization Method

As stated before, faulty SMs have higher capacitor voltages than healthy SMs under SM open-circuit failures. Hence, localization of faulty SMs is equivalent to identification of outliers. In statistics, an outlier is an observation point that is distant from other observations. Boxplots are an effective tool for outlier identification [29]. The idea of the proposed SM failure localization method evolves from outlier identification of the box plots. The SM failure localization method is executed with the following steps.

1) All SM capacitor voltages within the faulty arm are sorted in ascending order.
2) The first and third quartiles Q_1 and Q_3 are calculated based on the sorted SM voltage sequence.
3) The interquartile range (IQR) is calculated through $Q_3 - Q_1$.
4) The upper limit is calculated through the following equation:

$$V_{\mathrm{SM\_up}} = Q_3 + 1.5\mathrm{IQR}. \tag{10}$$

5) Each SM voltage is compared with $V_{\mathrm{SM\_up}}$. The SMs with capacitor voltages higher than $V_{\mathrm{SM\_up}}$ are identified as the faulty SMs.
6) The flowchart of the proposed SM failure localization method is displayed in Fig. 5.

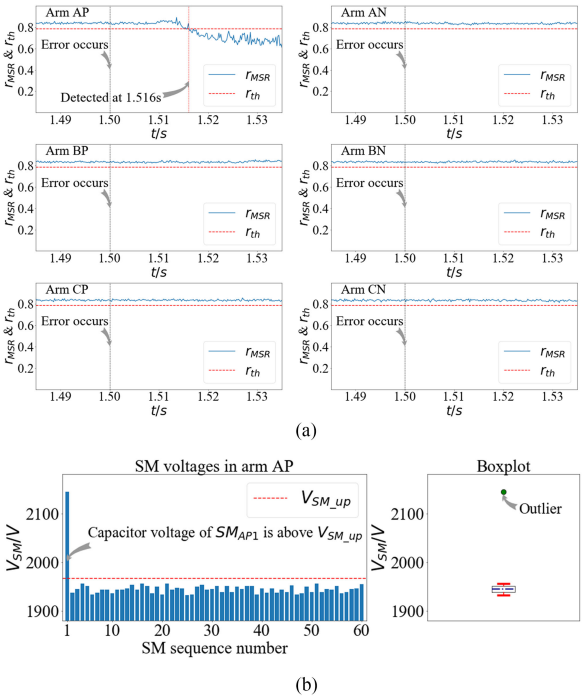

Fig. 8. Simulation results of single S_u open-circuit failure diagnosis. (a) SRT evaluation. (b) SM failure localization.

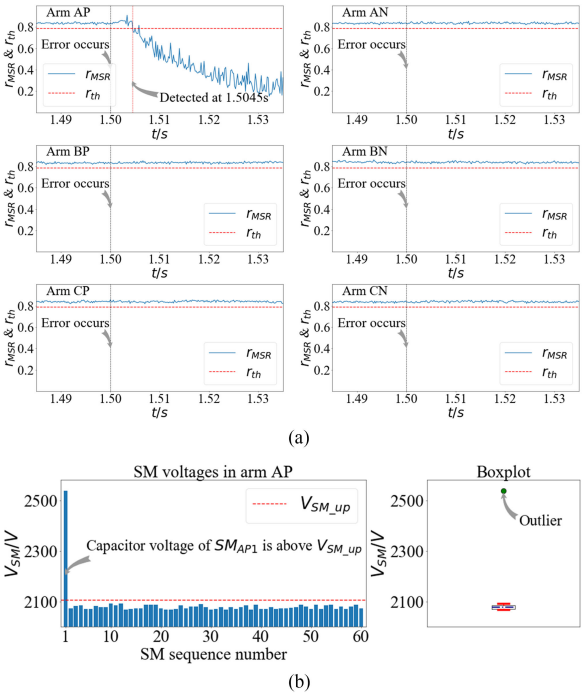

Fig. 9. Simulation results of single S_l open-circuit failure diagnosis. (a) SRT evaluation. (b) SM failure localization.

IV. Simulation Verification

In this section, the effectiveness of the proposed SM failure diagnosis method is assessed by simulation. A detailed model of a 61-level three-phase MMC is built in MATLAB/Simulink with the key parameters listed in Table IV. The fault characteristics of SM open-circuit failures are first demonstrated. The proposed method is then tested under different failure modes. Its effectiveness under parameter uncertainties is confirmed at last. A 60 × 100 random matrix is applied. S_{ram} in (9) is generated within [–1e–2, 1e–2] and ε in (7) is set to 0.95. The SRT algorithm is implemented based on Python. SM voltages are balanced with the sorting algorithm [22] and circulating currents are suppressed [30].

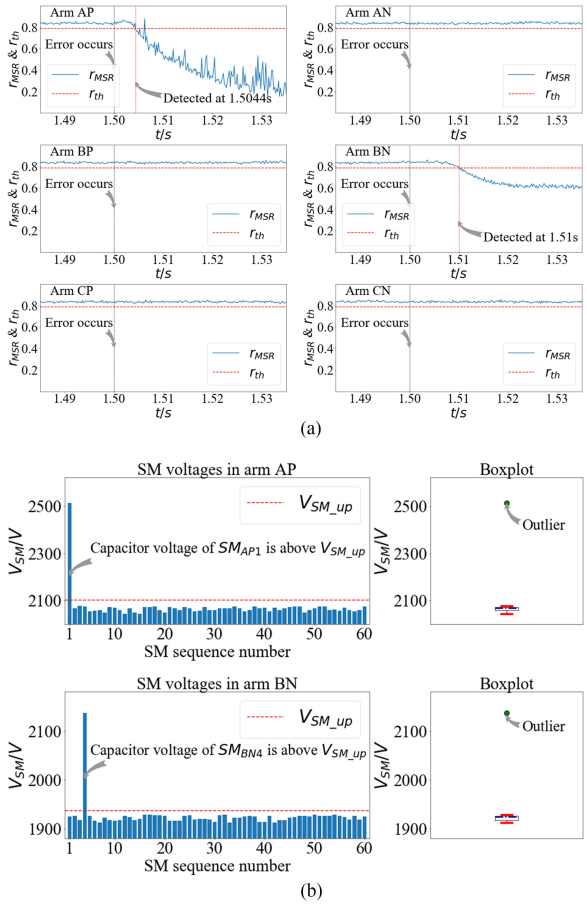

Fig. 10. Simulation results of multiple SM open-circuit failure diagnosis. (a) SRT evaluation. (b) SM failure localization.

A. Fault Characteristics of SM Open-Circuit Failures

To demonstrate the fault characteristics of SM open-circuit failures, one SM in arm AP is assumed to be damaged at 1.5 s. The resulting SM voltage waveforms under different types of SM open-circuit failures are shown in Fig. 6. Three different power factors ($\frac{\sqrt{2}}{2}, \frac{\sqrt{3}}{2}, 1$) are applied for each failure type. As can be seen from Fig. 6(a), the faulty SM is not discharged after 1.5 s and the voltage of the faulty SM stays at the highest point eventually under the S_u open-circuit failure regardless of the power factor. As for the S_l open-circuit failure, the SM voltage deviation between the faulty SM and the normal SMs tends to increase after 1.5 s under all three power factors as shown in Fig. 6(b). Under the S_u & S_l open-circuit failure, the faulty SM cannot be discharged, while its capacitor voltage increases gradually as shown in Fig. 6(c). The simulation results coincide with the analysis given in the previous section. Since the MMC

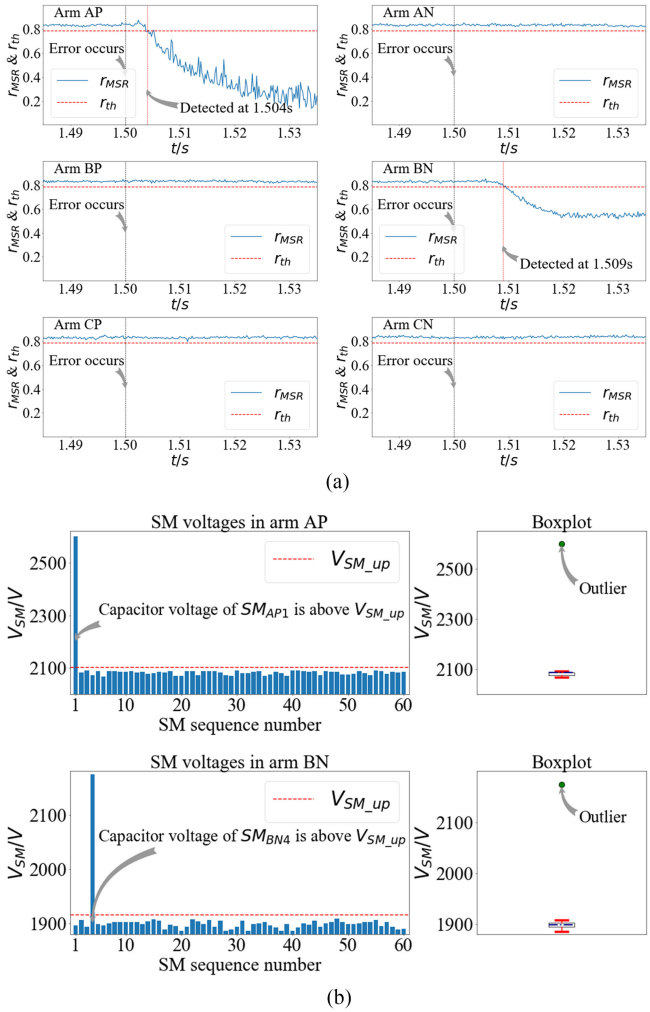

Fig. 11. Simulation results of multiple SM open-circuit failure diagnosis under parameter uncertainties. (a) SRT evaluation. (b) SM failure localization.

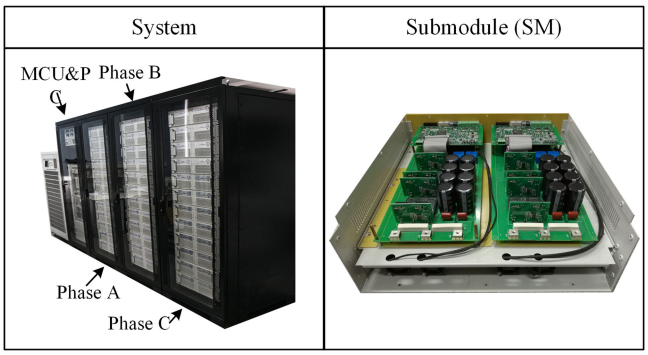

Fig. 12. Picture of the MMC prototype.

reveals similar fault characteristics under distinct power factors, the power factor will be fixed at one in the diagnosis without loss of generality.

B. SM Open-Circuit Failure Diagnosis

The robustness of the proposed method to transient process under normal operation is first demonstrated. It is then tested under different failure scenarios. Since S_u & S_l open-circuit failures are a combination of S_u open-circuit failures and S_l open-circuit failures, methods capable of detecting S_l open-circuit failures and S_l open-circuit failures are naturally compatible with the detection of S_u & S_l open-circuit failures. Considering this, only the diagnosis of S_u open-circuit failures and S_l open-circuit failures is discussed in this paper.

1) Case 1: Transient Under Normal Operation: In this case, the active transfer rating is switched from 1 to 0.5 p.u. at 1.5 s. Considering the symmetry of the MMC, arm AP is selected as a representative and the corresponding simulation result is shown in Fig. 7. As can be seen, r_{MSR} remains above r_{th} regardless of the transfer rating alternation. The transient process under normal operation triggers no false detection.

2) Case 2: Single SM Failure: The simulation results of single SM open-circuit failure diagnosis are shown in Fig. 8 (S_u open-circuit failure) and Fig. 9 (S_l open-circuit failure). One SM in the positive arm of phase A (SM_{AP1}) is assumed to be broken at 1.5 s. As can be seen from Figs. 8(a) and 9(a), r_{MSR} of arm AP exceeds the limit of r_{th} at 1.516 s under the S_u open-circuit failure, while at 1.5045 s under the S_l open-circuit failure. Meanwhile, r_{MSR} of other arms remains above r_{th}. The difference between the detection time of the S_u open-

TABLE V
KEY EXPERIMENTAL PARAMETERS

Item	Description	Value
S_{rated}	Rated apparent power	2 kVA
PF	Power factor	1
$u_{l\text{-}l}$	Line-line voltage (*rms*)	100 V
f	Grid frequency	50 Hz
U_{dc}	Rated dc voltage	400 V
C_{SM}	SM capacitance	2.4 mF
L_{Arm}	Arm inductance	15 mH
N_{SM}	Number of SMs/arm	12
f_s	Sampling frequency	5 kHz

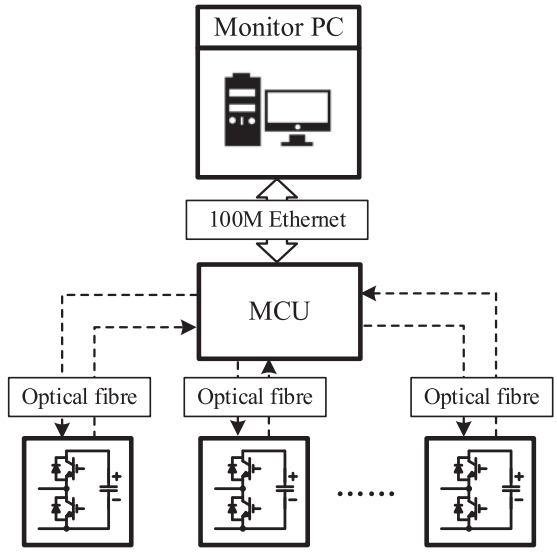

Fig. 13. Communication structure of the MMC prototype.

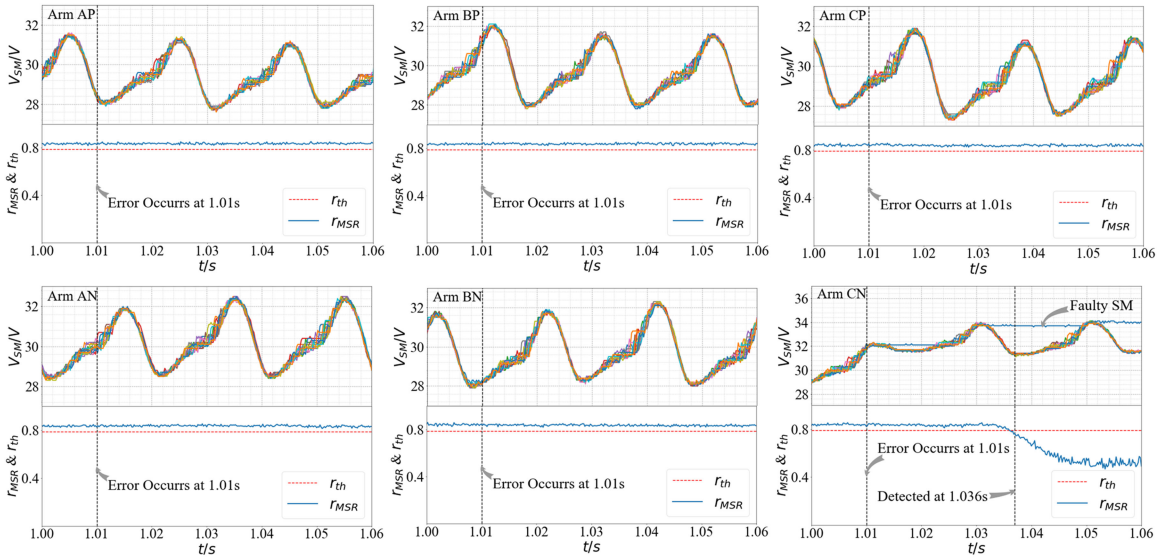

Fig. 14. Experimental results of single S_u open-circuit failure detection.

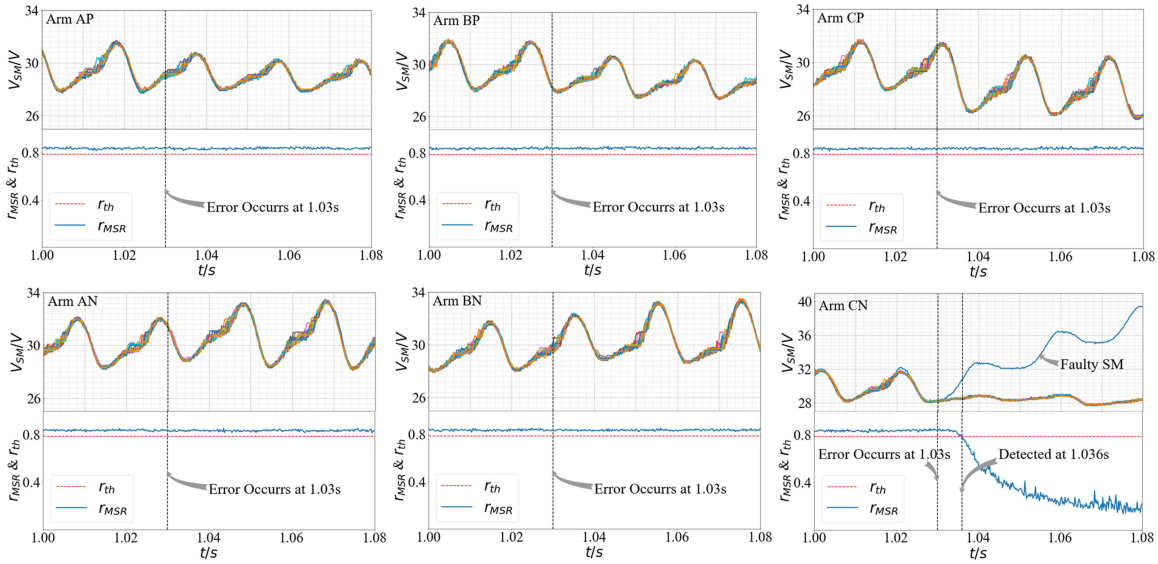

Fig. 15. Experimental results of single S_l open-circuit failure detection.

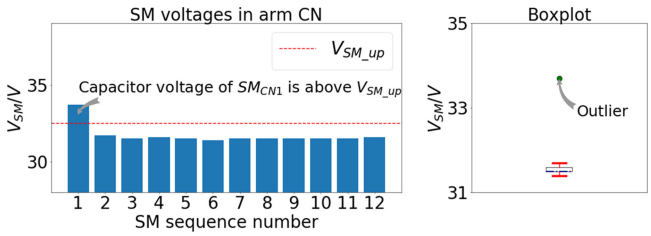

Fig. 16. Experimental results of single S_u open-circuit failure localization.

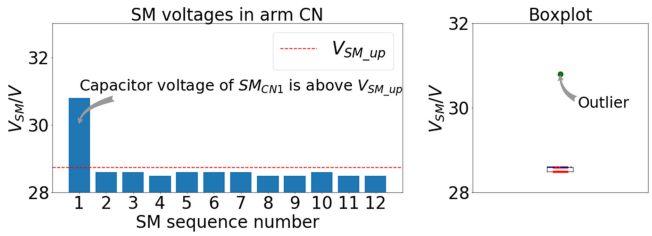

Fig. 17. Experimental results of single S_l open-circuit failure localization.

circuit failure and the S_l open-circuit failure is mainly due to current directions. As stated previously, positive SM currents have no impact on the faulty SMs under S_u open-circuit failures, like negative SM currents under S_l open-circuit failures. Therefore, the required detection time is directly related with the current direction at the failure instant. The SM failure localization results under the S_u open-circuit failure and the S_l open-circuit failure are presented in Figs. 8(b) and 9(b), respectively. From the bar plots on the left-hand side, the SM voltage of the faulty SM (SM_{AP1}) exceeds the upper limit $V_{\mathrm{SM\_up}}$ in both Figs. 8(b) and 9(b). Such a conclusion can also be drawn from the corresponding box plots on the right-hand side, where the volt-

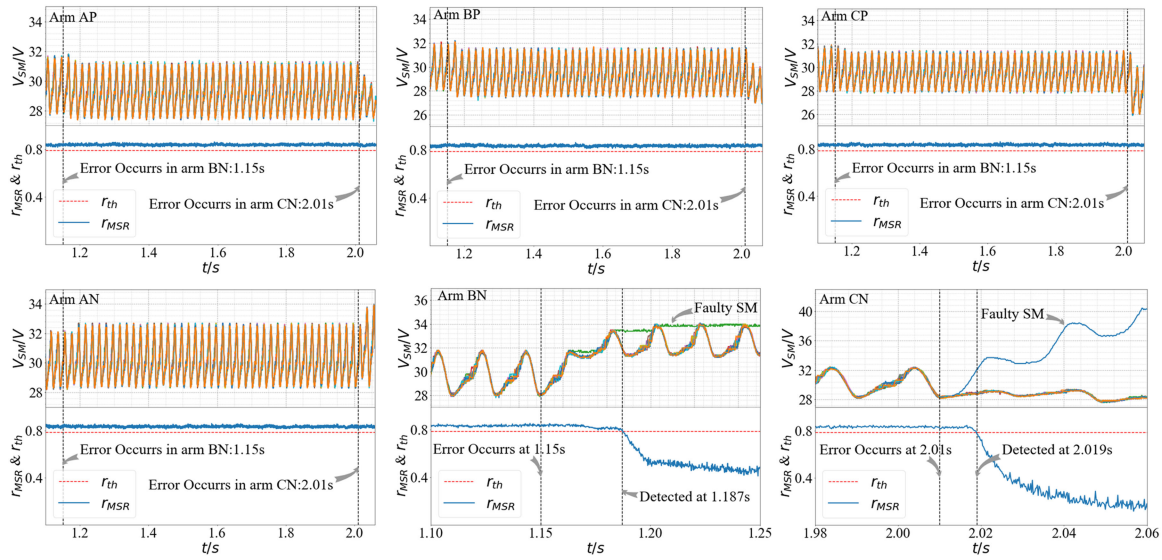

Fig. 18. Experimental results of multiple SM open-circuit failure detection.

age of SM_{AP1} is identified as an outlier. Therefore, the proposed method accomplishes single SM open-circuit failure detection and localization.

3) Case 3: Multiple SM Failures: The simulation results of multiple SM open-circuit failure diagnosis are shown in Fig. 10. An S_l open-circuit failure is triggered on SM_{AP1} while an S_u open-circuit failure is imposed on SM_{BN4} at 1.5 s. As can be seen from Fig. 10(a), the proposed method detects the open-circuit failure in SM_{AP1} and SM_{BN4} at 1.5044 and 1.51 s, respectively. As for SM failure localization, both SM_{AP1} and SM_{BN4} are correctly identified with the proposed localization method as shown in Fig. 10(b) with significantly larger capacitor voltages than $V_{\mathrm{SM\_up}}$. In general, the proposed method manages to detect and locate multiple SM open-circuit failures in the MMC.

4) Case 4: Parameter Uncertainties: To demonstrate the immunity to parameter uncertainties of the proposed failure diagnosis method, distortions have been taken on arm inductance and SM capacitance with $L'_{\mathrm{Arm}} = 1.2L_{\mathrm{Arm}}$ and $C'_{\mathrm{SM}} = 0.8C_{\mathrm{SM}}$. A similar multiple failure configuration is applied as in Case 3. The simulation results are presented in Fig. 11. The proposed method manages to detect the failure in SM_{AP1} (SM_{BN4}) 4 ms (9 ms) after occurrence and correctly identifies the faulty SMs. Such simulation results establish the robustness of the proposed method in terms of parameter uncertainties.

V. Experimental Verification

The proposed SM open-circuit failure diagnosis method is verified on a three-phase MMC prototype in the laboratory. The MMC prototype consists of 12SMs within each arm and is designed under a rated power of 30 kW and a rated dc voltage of 2 kV. A picture of the MMC prototype is presented in Fig. 12. The prototype comprises of four cabinets: one control cabinet containing a main control unit (MCU) and a monitor PC and three SM cabinets containing the stacked SMs of each phase. Key experimental parameters are given in Table V. A dc power source is used to support the dc voltage, while the ac output is connected to a grid simulator. The active power and dc voltage are set to 2 kW and 400 V, based on safety limits. The communication structure of the MMC prototype is presented in Fig. 13. A 5 kHz sampling frequency is used experimentally, as in the simulations in the previous section. The SM voltage samples are transferred to the MCU via parallel optical fibers and then to the monitor PC for state evaluation. To enable sufficient data transmission capability, a communication module based on 100M Ethernet is embedded in the MCU. The sampled SM capacitor voltages are transferred to the monitor PC via the Ethernet-based communication module with a bit rate of 8 Mb/s. A 60×100 random matrix is applied for failure detection in the experiment, where each sampling value of the 12SMs is reused five times in random matrix generation. The SRT evaluations demonstrated in this section are executed offline with the sampling data.

1) Case 1: Single SM Failure

The experimental results of single S_u open-circuit failure detection are presented in Fig. 14. An error is activated at 1.01 s on SM_{CN1}. The upper graph in each subplot in Fig. 14 is the SM capacitor voltages within one arm, while the lower plot depicts the corresponding r_{MSR}. As can be seen, r_{MSR} of arm CN falls below the limit of r_{th} 26 ms after failure occurrence, while r_{MSR} of other arms is unaffected by the fault and remains above r_{th} after 1.01 s. This indicates successful failure detection. The SM voltage waveforms of arm CN also coincide with the fault characteristics analyzed in the previous section. The experimental results of single S_l open-circuit failure detection are presented in Fig. 15. An error is triggered at 1.03 s on SM_{CN1}. As can be seen, the proposed method detects the SM failure in arm CN 6 ms after occurrence.

The experimental results of S_u open-circuit failure and S_l open-circuit failure localization are shown in Figs. 16 and 17, respectively. SM_{CN1} is correctly identified as the faulty SM with a larger SM voltage than $V_{\mathrm{SM\_up}}$ in both cases. Similar conclusion can be drawn via the boxplot on the right-hand side, where the SM voltage of SM_{CN1} is regarded as an out-

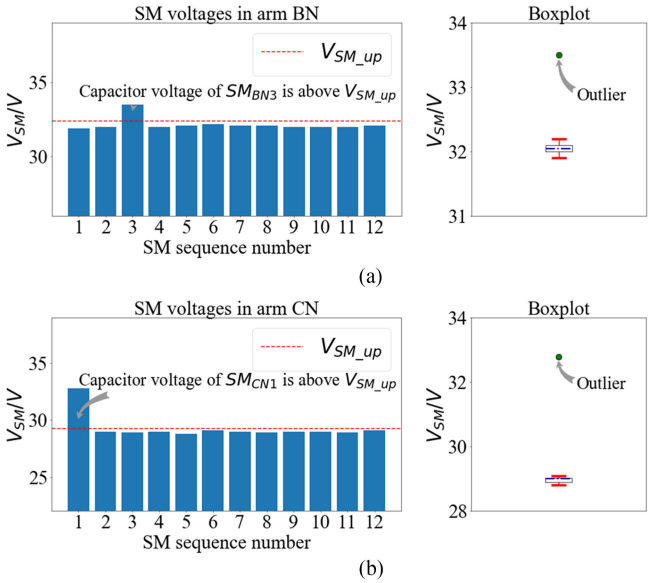

Fig. 19. Experimental results of multiple SM open-circuit failure localization. (a) Arm BN. (b) Arm CN.

lier. Longer detection time is required compared with the same case in the 120 MW simulation, which is mainly due to the relatively slower formation of deviations as a result of smaller currents.

2) Case 2: Multiple SM Failures

The experimental results of multiple SM open-circuit failure detection are presented in Fig. 18. An S_u open-circuit failure is activated on SM_{BN3} at 1.15 s, then an S_l open-circuit failure is triggered on SM_{CN1} at 2.01 s. As can be seen, r_{MSR} of arm BN and arm CN falls below r_{th} at 1.87 and 2.019 s, respectively. Meanwhile, r_{MSR} of other arms remains above r_{th} during the whole time and thus no false alarm is generated. The experimental results of multiple SM open-circuit failure localization are presented in Fig. 19. In Fig. 19(a), SM_{BN3} is correctly identified as the faulty with a larger SM voltage than $V_{\mathrm{SM\_up}}$. In Fig. 19(b), the failure in SM_{CN1} is also correctly located with the proposed method. The experimental results establish the capability of the proposed method in detecting and locating multiple SM open-circuit failures even if the faulty SMs are in different arms.

VI. Conclusions

In this paper, an SM open-circuit failure diagnosis method has been proposed for MMCs. Two steps are executed in the proposed method: Failure detection then faulty SM localization. A failure detection method based on the SRT is proposed along with a statistical-analysis-based failure localization method. The superiorities of the proposed diagnosis method include the following.

1) No estimators are applied which ensures robustness in terms of parameter uncertainties and hence good generalization ability.
2) No extra sensors are required. The implementation is based on SM voltages which are already available as measurement inputs to the control system. Hence, no additional cost is introduced.
3) The SM failure diagnosis method is capable of detecting both single and multiple SM failures even if the faulty SMs are in different arms.
4) The method enables fast failure detection and localization (no more than 10 ms at 120 MW and no more than 40 ms at 2 kW).

The effectiveness of the proposed method has been established by simulation on a 61-level MMC model in MATLAB/Simulink and experimentally on a 13-level MMC. The proposed method accomplishes failure detection and localization tasks under both single and multiple SM failures. Nevertheless, further modifications are required on the current execution process of the proposed method to enable efficient online diagnosis. The modifications could be made on hardware (e.g., using a powerful workstation as the monitor PC) or software (e.g., applying the multithreading technology), which calls for further research and improvements.

References

[1] A. Nami, J. Liang, F. Dijkhuizen, and G. D. Demetriades, "Modular multilevel converters for HVDC applications: Review on converter cells and functionalities," *IEEE Trans. Power Electron.*, vol. 30, no. 1, pp. 18–36, Jan. 2015.
[2] H. M. P. and M. T. Bina, "A transformerless medium-voltage STATCOM topology based on extended modular multilevel converters," *IEEE Trans. Power Electron.*, vol. 26, no. 5, pp. 1534–1545, May 2011.
[3] J. Mei, B. Xiao, K. Shen, L. M. Tolbert, and J. Y. Zheng, "Modular multilevel inverter with new modulation method and its application to photovoltaic grid-connected generator," *IEEE Trans. Power Electron.*, vol. 28, no. 11, pp. 5063–5073, Nov. 2013.
[4] R. Marquardt, "Modular multilevel converter: A universal concept for HVDC-Networks and extended DC-Bus-applications," in *Proc. Int. Power Electron. Conf.*, Jun. 2010, pp. 502–507.
[5] A. Lesnicar and R. Marquardt, "An innovative modular multilevel converter topology suitable for a wide power range," in *Proc. IEEE Bologna Power Tech Conf.*, Jun. 2003, vol. 3.
[6] M. Hagiwara and H. Akagi, "Control and experiment of pulse width-modulated modular multilevel converters," *IEEE Trans. Power Electron.*, vol. 24, no. 7, pp. 1737–1746, Jul. 2009.
[7] S. Rohner, S. Bernet, M. Hiller, and R. Sommer, "Modulation, losses, and semiconductor requirements of modular multilevel converters," *IEEE Trans. Power Electron.*, vol. 57, no. 8, pp. 2633–2642, Aug. 2010.
[8] S. Debnath, J. Qin, B. Bahrani, M. Saeedifard, and P. Barbosa, "Operation, control, and applications of the modular multilevel converter: A review," *IEEE Trans. Power Electron.*, vol. 30, no. 1, pp. 37–53, Jan. 2015.
[9] M. Guan and Z. Xu, "Modeling and control of a modular multilevel converter-based HVDC system under unbalanced grid conditions," *IEEE Trans. Power Electron.*, vol. 27, no. 12, pp. 4858–4867, Dec. 2012.
[10] M. Saeedifard and R. Iravani, "Dynamic performance of a modular multilevel back-to-back HVDC system," *IEEE Trans. Power Del.*, vol. 25, no. 4, pp. 2903–2912, Oct. 2010.
[11] M. A. Perez, S. Bernet, J. Rodriguez, S. Kouro, and R. Lizana, "Circuit topologies, modeling, control schemes, and applications of modular multilevel converters," *IEEE Trans. Power Electron.*, vol. 30, no. 1, pp. 4–17, Jan. 2015.
[12] F. Richardeau and T. T. L. Pham, "Reliability calculation of multilevel converters: Theory and applications," *IEEE Trans. Ind. Electron.*, vol. 60, no. 10, pp. 4225–4233, Oct. 2013.
[13] H. J. Schulze, F. J. Niedernostheide, F. Pfirsch, and R. Baburske, "Limiting factors of the safe operating area for power devices," *IEEE Trans. Electron Devices*, vol. 60, no. 2, pp. 551–562, Feb. 2013.
[14] M. Ciappa, "Selected failure mechanisms of modern power modules," *Microelectron. Rel.*, vol. 42, nos. 4/5, pp. 653–667, 2012.
[15] B. Lu and S. K. Sharma, "A literature review of IGBT fault diagnostic and protection methods for power inverters," *IEEE Trans. Ind. Appl.*, vol. 45, no. 5, pp. 1770–1777, Jul. 2009.

[16] S. Shao, P. W. Wheeler, J. C. Clare, and A. J. Watson, "Fault Detection for modular multilevel converters based on sliding mode observer," *IEEE Trans. Power Electron.*, vol. 28, no. 11, pp. 4867–4872, Nov. 2013.
[17] S. Shao, A. J. Watson, J. C. Clare, and P. W. Wheeler, "Robustness analysis and experimental validation of a fault detection and isolation method for the modular multilevel converter," *IEEE Trans. Power Electron.*, vol. 31, no. 5, pp. 3794–3805, May 2016.
[18] Q. Yang, J. Qin, and M. Saeedifard, "Analysis, detection, and location of open-switch submodule failure in a modular multilevel converter," *IEEE Trans. Power Del.*, vol. 31, no. 1, pp. 155–164, Feb. 2016.
[19] F. Deng, Z. Chen, M. R. Khan, and R. Zhu, "Fault Detection and localization method for modular multilevel converters," *IEEE Trans. Power Electron.*, vol. 30, no. 5, pp. 2721–2732, May 2015.
[20] B. Li, S. Shi, B. Wang, G. Wang, W. Wang, and D. Xu, "Fault Diagnosis and tolerant control of single IGBT open-circuit failure in modular multilevel converters," *IEEE Trans. Power Electron.*, vol. 31, no. 4, pp. 3165–3176, Apr. 2016.
[21] R. Picas, J. Zaragoza, J. Pou, and S. Ceballos, "Reliable Modular multilevel converter fault detection with redundant voltage sensor," *IEEE Trans. Power Electron.*, vol. 32, no. 1, pp. 39–51, Jan. 2017.
[22] Q. Tu and Z. Xu, "Impact of sampling frequency on harmonic distortion for modular multilevel converter," *IEEE Trans. Power Del.*, vol. 26, no. 1, pp. 298–306, Jan. 2011.
[23] X. He, Q. Ai, R. C. Qiu, W. Huang, L. Piao, and H. Liu, "A Big data architecture design for smart grids based on random matrix theory," *IEEE Trans. Smart Grid*, vol. 8, no. 2, pp. 674–686, Mar. 2017.
[24] X. Xu, X. He, Q. Ai, and R. C. Qiu, "A correlation analysis method for power systems based on random matrix theory," *IEEE Trans. Smart Grid*, vol. 8, no. 4, pp. 1811–1820, Jul. 2017.
[25] A. Guionnet, M. Krishnapur, and O. Zeitouni, "The single ring theorem," *Ann. Math.*, vol. 174, pp. 1189–1217, 2011.
[26] F. Benaych-Georges and J. Rochet, "Outliers in the single ring theorem (Report)," *Probab. Theory Related Fields*, vol. 165, nos. 1/2, pp. 313–363, 2016.
[27] W. Zhou *et al.*, "Common-mode voltage injection-based nearest level modulation with loss reduction for modular multilevel converters," *IET Renewable Power Gener.*, vol. 10, no. 6, pp. 798–806, 2016.
[28] D. Freedman, *Statistics*. New York, NY, USA: W. W. Norton & Company, 1991.
[29] J. W. Tuckey, *Exploratory Data Analysis*. Reading, MA, USA: Addison-Wesley, 1977.
[30] Q. Tu, Z. Xu, and L. Xu, "Reduced switching-frequency modulation and circulating current suppression for modular multilevel converters," *IEEE Trans. Power Del.*, vol. 26, no. 3, pp. 2009–2017, Jul. 2011.

Weihao Zhou was born in Sichuan, China, in 1991. He received the B.Sc. degree from Zhejiang University, Hangzhou, China, in 2013, where he is currently working toward the Ph.D. degree in electrical engineering.

From February 2017 to October 2017, he was a Research Intern with GE Global Research Center, Shanghai, China. His research interests include control and diagnosis of modular multilevel converters and data science application in power electronics.

Jing Sheng was born in Anhui, China, in 1993. He received the B.S. degree from the College of Electrical Engineering, Zhejiang University, Hangzhou, China, in 2017, where he is currently working toward the Ph.D. degree in electrical engineering.

His research interests include control of modular multilevel converters.

Haoze Luo (M'15) received the B.S. and M.S. degrees from Hefei University of Technology, Hefei, China, in 2008 and 2011, respectively, and the Ph.D. degree from Zhejiang University, Hangzhou, China, in 2015.

He is currently working as a Postdoc with the Department of Energy Technology, Aalborg University, Aalborg, Denmark. From January to April 2015, he was a Visiting Researcher with Newcastle University, Newcastle upon Tyne, U.K. His research interests include testing, failure analysis, and reliability assessment of semiconductor power devices.

Wuhua Li (M'09) received the B.Sc. and Ph.D. degrees in applied power electronics and electrical engineering from Zhejiang University, Hangzhou, China, in 2002 and 2008, respectively.

From 2004 to 2005, he was a Research Intern, and from 2007 to 2008, a Research Assistant with GE Global Research Center, Shanghai, China. From 2008 to 2010, he joined the College of Electrical Engineering, Zhejiang University, as a Postdoctor. In 2010, he was promoted as an Associate Professor. Since 2013, he has been a Full Professor with Zhejiang University. From 2010 to 2011, he was a Ryerson University Postdoctoral Fellow with the Department of Electrical and Computer Engineering, Ryerson University, Toronto, ON, Canada. His research interests include power devices, converter topologies and advanced controls for high power energy conversion systems. He has authored and coauthored more than 200 peer-reviewed technical papers and holds more than 30 issued/pending patents.

Dr. Li was the recipient of the 2012 Delta Young Scholar from Delta Environmental & Educational Foundation, the 2012 Outstanding Young Scholar from National Science Foundation of China (NSFC), the 2013 Chief Youth Scientist of National 973 Program, and the 2014 Young Top-Notch Scholar of National Ten Thousand Talent Program, for his excellent teaching and research contributions. He was also the recipient of the National Natural Science Award and four Scientific and Technological Achievement Awards from Zhejiang Provincial Government and the State Educational Ministry of China. He was appointed as the Most Cited Chinese Researchers by Elsevier since 2014. He serves as the Associate Editor of *Journal of Emerging and Selected Topics in Power Electronics*, *IET Power Electronics*, *CSEE Journal of Power and Energy Systems*, *Proceedings of the Chinese Society for Electrical Engineering*, Guest Editor of *IET Renewable Power Generation* for Special Issue "DC and HVDC system technologies," and a Member of Editorial Board for *Journal of Modern Power System and Clean Energy*.

Xiangning He (M'95–SM'96–F'10) received the B.Sc. and M.Sc. degrees from Nanjing University of Aeronautical and Astronautical, Nanjing, China, in 1982 and 1985, respectively, and the Ph.D. degree from Zhejiang University, Hangzhou, China, in 1989.

From 1985 to 1986, he was an Assistant Engineer with the 608 Institute of Aeronautical Industrial General Company, Zhuzhou, China. From 1989 to 1991, he was a Lecturer with Zhejiang University. In 1991, he obtained a Fellowship from the Royal Society of U.K., and conducted research in the Department of Computing and Electrical Engineering, Heriot-Watt University, Edinburgh, U.K., as a Postdoctoral Research Fellow for two years. In 1994, he joined Zhejiang University as an Associate Professor. Since 1996, he has been a Full Professor with the College of Electrical Engineering, Zhejiang University. He was the Director of the Power Electronics Research Institute, the Head of the Department of Applied Electronics, the Vice Dean of the College of Electrical Engineering, and he is currently the Director of the National Specialty Laboratory for Power Electronics, Zhejiang University. His research interests include power electronics and their industrial applications.

Dr. He was appointed as the IEEE Distinguished Lecturer by the IEEE Power Electronics Society in 2011. He is also a Fellow of the Institution of Engineering and Technology (formerly IEE), U.K.